Possible Regulatory Role for the Histidine-Rich Loop in the Zinc Transport Protein, ZnuA[†,‡]

Baoxian Wei,[§] Amelia M. Randich,[§] Maitrayee Bhattacharyya-Pakrasi,[||] Himadri B. Pakrasi,[||] and Thomas J. Smith*[,§]

Donald Danforth Plant Science Center, 975 North Warson Road, St. Louis, Missouri 63132, and Department of Biology, Campus Box 1137, Washington University, St. Louis, Missouri 63130

Received April 23, 2007; Revised Manuscript Received May 29, 2007

ABSTRACT: A number of bacterial metal transporters belong to the ABC transporter family. To better understand the structural determinants of metal selectivity of one such transporter, we previously determined the structure of the periplasmic domain of a zinc transporter, ZnuA, from *Synechocystis* 6803 and found that ZnuA binds zinc via three histidines. Unique to these ABC zinc transporters, ZnuA has a highly charged and mobile loop that protrudes from the protein in the vicinity of the metal binding site that we had suggested might facilitate zinc acquisition. To further examine the function of this loop, the structure and zinc binding properties of two ZnuA variants were determined. When the loop is entirely deleted, zinc still binds to the three histidines. However, unlike what was suggested from the structure of a similar solute binding protein, TroA, release of zinc occurs concomitantly with large conformational changes in two of the three chelating histidines. These structural results combined with isothermal titration calorimetry data demonstrate that there are at least two classes of zinc binding sites: the high-affinity site in the cleft between the two domains and at least one additional site on the flexible loop. This loop has approximately 100-fold weaker affinity for zinc than the high-affinity zinc binding site, and its deletion does not affect the high-affinity site. From these results, we suggest that this region might be a sensor for high periplasmic levels of zinc.

Bacterial survival and proliferation in the environment as well as within various hosts are critically dependent on the uptake and sequestration of transition metals such as manganese, zinc, and iron. Zinc is an essential element in all organisms and is abundant in the biosphere. Its Lewis acidity, flexible coordination geometry, and rapid ligand exchange properties have led to zinc being the metal of choice in over 300 biological proteins. Although an essential metal in cell growth, zinc is stringently regulated in the cell since high concentrations are toxic to a number of cellular functions. To acquire sufficient amounts of zinc for metabolism, cells have evolved several types of proteins that bind and transport zinc (*1*). Zinc transport across the plasma membranes of various bacterial species has been well investigated. Intracellular levels of zinc in bacteria are maintained within strict limits by the activities of several transport mechanisms involving both the uptake and efflux of zinc (reviewed in refs *2* and *3*).

A class of ATP-binding cassette-type (ABC[1]-type) transport systems is involved in the uptake of transition metal ions. This system has several homologues in various Gram-positive and Gram-negative bacteria that are responsible for the transport of divalent metal cations such as Mn^{2+} and Zn^{2+}, particularly at low extracellular levels of these metals (*1*, *2*, *4*). The ABC-type binding proteins from a number of bacteria have been grouped into clusters according to their sequence homologies and the metal ligand identities (*5*). On this basis, the zinc transporter ZnuA from *Escherichia coli* (*2*) and *Synechocystis* 6803 (*6*), the manganese transporter PsaA from *Streptococcus pneumoniae* (*7*), and the proposed zinc transporter TroA from *Treponema pallidum* (*8*−*10*) have been placed in a newly defined "cluster 9" (*1*). First identified in *E. coli*, the *znu* (*z*in*c u*ptake) system has been shown to be important for scavenging and transport of Zn^{2+} (*11*). Inactivation of genes that encode homologues of *znuA* has resulted in decreased growth rates and virulence in several pathogenic bacteria (*7*, *12*, *13*). In *Synechocystis* 6803, the *znu* operon includes the *znuA*, *znuB*, and *znuC* genes that encode the periplasmic Zn binding protein, the integral membrane protein component, and the cytoplasmic ABC cassette domain, respectively (Bhattacharyya-Pakrasi et al., submitted for publication).

[†] This work was supported by a grant from the U.S. Environmental Protection Agency (EPA-X-83220101 to T.J.S.), the National Science Foundation (EF0425749 to M.B.-P.), and the Membrane Biology EMSL Scientific Grand Challenge project at the W. R. Wiley Environmental Molecular Sciences Laboratory, a national scientific user facility sponsored by the U.S. Department of Energy's Office of Biological and Environmental Research (BER) program located at Pacific Northwest National Laboratory.

[‡] X-ray coordinates have been deposited in the Protein Data Bank of the ZnuA deletion mutant in the presence and absence of bound zinc (2OV3 and 2OV1, respectively) and will be released upon publication.

* Corresponding author. Telephone: (314) 587-1451. Fax: (314) 587-1551. E-mail: tsmith@danforthcenter.org.

[§] Donald Danforth Plant Science Center.

[||] Washington University.

[1] Abbreviations: ABC, ATP binding cassette; SBP, solute binding protein; ITC, isothermal titration calorimetry; IPTG, isopropyl 1-thio-D-galactopyranoside; PBS, phosphate-buffered saline; PCR, polymerase chain reaction; CCD, charge coupling device.

10.1021/bi700763w CCC: $37.00
Published on Web 07/06/2007

Table 1: Primers Used for ZnuA Mutagenesis

1	5′-GGAATTCCAGCCCGCTGTTGAACAGGT-3′ (forward)
2	5′-CTTATCGGTATAGGGGCCGTCGGCCATTTCCAGGGGGGTTATGCCTTG-3′ (reverse)
3	5′- GCCGACGGCCCCTATACCGATAAGATGGTGGCGGATCCCCACATTTGG-3′ (forward)
4	5′-CCGCTCGAGTTAGGGCTGGGCACTGTTAG-3′ (reverse)
5	5′-GGAATTCCAGCCCGCTGTTGAACAGGT-3′ (forward)
6	5′-GAGTCGACCCGGCATTTCCAGGGGTGTTATGCCTTGGGCCG-3′ (reverse)
7	5′-ACGCGTCGACTCATGGTGGCGGATCCCCACATTTGG-3′ (forward)
8	5′-CCGCTCGAGTTAGGGCTGGGCACTGTTAG-3 (reverse)

In previously published work, we described the structure of the periplasmic solute binding protein (SBP), ZnuA, from *Synechocystis* 6803 with zinc bound at 1.9 Å (*14*). The overall fold was very similar to that of the SBPs from the two transition metal ABC permeases PsaA and TroA. However, we found that ZnuA has a novel three-histidine zinc-chelating site, and we proposed that this limited chelating environment might favor the binding of zinc over other metals such as manganese. However, recent structures of ZnuA from *E. coli* identified an additional glutamate in the binding pocket (*15*, *16*). Therefore, the structural determinants of metal specificity, at least for *E. coli* ZnuA, are unclear. Unique to these zinc transport proteins, ZnuA has a flexible loop near the entrance to the metal binding site that is rich in histidine and acidic amino acids. Since similar motifs are found in other types of zinc transporters, we proposed that such loops act as zinc chaperones to facilitate the sequestering of zinc around the metal binding site. Very recent studies suggested that this loop might be acting like a HIS tag and facilitate binding of the protein to a nickel affinity column (*16*).

The possible functions of this unusual and flexible loop are further examined in this current study. Two variants of ZnuA were constructed: one with the entire loop deleted and a second with half of the loop removed. The atomic structures and zinc binding properties of these various constructs were examined. The loop clearly binds several zinc ions but with ~100 lower affinity than the main, high-affinity site. This high-affinity site is unaffected by the deletion of the loop, and therefore the loop may not be playing a major role in zinc sequestration. Therefore, we suggest that perhaps this loop is involved in sensing high levels of periplasmic zinc and shutting down zinc import before transcription has a chance to downregulate expression of this high-affinity transport complex.

MATERIALS AND METHODS

Oligonucleotide-Directed Mutagenesis. The DNA fragment encoding ZnuA (residues 28−339) was digested from pET41a/ZnuA, which was created from genomic DNA as previous described (*14*), with *Eco*RI and *Xho*I and ligated into the pGEX-4T-1 (Amersham Pharmacia Biotech) vector in-frame with the N-terminal glutathione *S*-transferase gene (GST). The resulting vector was used for wild-type ZnuA expression.

Site-directed mutagenesis for the half-loop truncation of ZnuA (Δ157−173) was performed using overlapping PCR, two sets oligonucleotides (primers 1−4, Table 1), and the pGEX-4T-1/ZnuA plasmid as template. The overlapping PCR product was purified and digested with *Eco*RI and *Xho*I and cloned into the pEGX-4T-1 vector. The resulting half-loop mutant (Δ157−173 ZnuA) was confirmed by DNA sequencing. The final protein sequence for this region is shown in Table 2.

Table 2: Sequences of the Flexible Loop Deletion Mutants of ZnuA[a]

```
(Δ138-173)ZnuA: LEM--PGRL--------------------------------MVA
(Δ158-173)ZnuA: LEM--EKHDHSHGEEEGHDDHSHDGPYTDK------------MVA
wtZnuA:         LEM--EKHDHSHGEEEGHDDHSHDGHDHGSESEKEKAKGAL--MVA
                     |                  |              |
                    138                158            173
```

[a] Shown here are the sequences of the flexible loop in the three forms of ZnuA. The middle segment represents those residues that were disordered in the structure of the wild-type ZnuA (*14*). The short segments that are underlined represent residues that were used as linker regions in the constructs and are not found in the wild-type sequence. Numbering used for all constructs corresponds to the wild-type sequence.

The truncation of the entire flexible loop (Δ138−173 ZnuA) was performed in two steps. The DNA fragment encoding ZnuA residues 28−137 was first amplified by PCR from the pEGX-4T-1/ZnuA plasmid using primers 5 and 6 (Table 1). The purified PCR product was digested with *Eco*RI and *Sal*I and ligated into the pGEX-4T-1 vector. The DNA fragment encoding ZnuA residues 174−339 was then amplified by PCR from pGEX-4T-1/ZnuA using forward and reverse primers 7 and 8 (Table 1). The PCR product was digested with *Sal*I and *Xho*I and subsequently cloned into pGEX-4T-1/ZnuA-28−137. The resulting vector was sequenced for confirmation. The final protein sequences of loop truncation mutants are shown in Table 2.

Mutagenesis and Protein Expression. The purification of recombinant wild-type and mutant ZnuA was performed as described previously (*14*) with minor modifications. Briefly, *E. coli* BL21(DE3) pLysS cells transfected with the ZnuA/pGEX-4T-1, Δ158−173 ZnuA/pGEX-4T-1, or Δ138−173 ZnuA/pGEX-4T-1 vector were grown at 37 °C in 2-YT medium containing both ampicillin (50 μg/mL) and chloramphenicol (34 μg/mL). When the optical density at 600 nm reached ~0.6, isopropyl 1-thio-D-galactopyranoside (IPTG, Inalc, Italy) was added to a final concentration of 0.4 mM to induce protein expression. The cultures were then grown at 37 °C for another 3.5 h, and the cells were harvested by centrifugation (4000*g*, 30 min). The cells were resuspended in 10 mM PBS (pH 7.4) and disrupted by a French press. The cell debris was removed by centrifugation at 15000*g* for 45 min.

The supernatant was applied to a column of glutathione−agarose (Sigma-Aldrich, St. Louis), and the column was washed with PBS. The proteins were eluted with a 0−10 mM linear gradient of glutathione, buffered to pH 8.0. Fractions were pooled, and thrombin (Sigma-Aldrich, St. Louis, MO) was added to remove the GST tag. The digested

solutions were dialyzed against PBS and passed back over the glutathione−agarose column to remove GST and undigested fusion protein. The purity of the proteins was verified by SDS−polyacrylamide gel electrophoresis.

Preparation of Apo Wild-Type and Mutant ZnuA. Zinc was removed from wild-type and mutant ZnuA as previously described (*10*) with minor modifications. Purified ZnuA protein was diluted to a concentration of 2 mg/mL and then dialyzed against 0.1 M sodium acetate (pH 4.6) and 10 mM 1,10-phenanthroline overnight with four buffer changes. Atomic absorption spectroscopy was used to confirm that the zinc had been removed from the protein.

Crystallization of the Δ138−173 ZnuA Mutant. Δ138−173 ZnuA was concentrated to 15 mg/mL using Amicon Centricons and crystallized using the vapor diffusion method at room temperature. The reservoir solution contained 100 mM ADA, pH 6.5, and 1.8−2.0 M ammonium sulfate. Crystals grew to dimensions of 0.2 × 0.3 × 0.1 mm.

Diffraction Data Collection and Structure Determination. Diffraction data from crystals of the mutated version of ZnuA were collected using a single frozen crystal at ~100 K using an Oxford cryosystem and a Proteum R Smart 6000 CCD detector connected to a Bruker-Nonius FR591 rotating anode generator. To prepare for freezing, crystals were first placed in mother liquor, and then glycerol was added in 4% (v/v) increments up to a final concentration of 24%. Soaking times for each step were about 15 min. A total of 500 image frames were collected using an oscillation angle of 0.5° and an exposure time of 2 min per frame. While reflections were observed to a resolution of 2.0 Å, data were integrated and scaled to 2.5 Å. Diffraction intensities were integrated, merged, and scaled using the Proteum software suite. The program SHEL-X was used to independently validate the space group. The crystals belong to the space group $C222_1$ with unit cell dimensions of $a = 62.58$ Å, $b = 76.503$ Å, and $c = 127.15$ Å. From V_m calculations, it was determined that there was one molecule in each asymmetric unit ($V_m = 2.49$ Å^3/Da).

The structure was determined by molecular replacement using the program MOLREP (*17*) and the previously published structure of the zinc-bound form of ZnuA (*14*). The best solution maximum in the cross-rotation function was ~20σ with the next best solution being ~6σ. The best rotation function solution then yielded a translation function *R*-factor of 44.9% using data between 10 and 3 Å compared to 61% for the next best solution. CNS (*18*) was used for all subsequent refinement, and the program O (*19*) was used to make adjustments to the model. The model was subjected to cycles of simulated annealing, energy minimization, and *B*-factor refinement. The program PROCHECK (*20*) was used to monitor the stereochemical parameters during refinement. Table 3 summarizes the final refinement statistics. Upon refinement of this structure, it was apparent that zinc was not present as it had been in the case of full-length ZnuA (*14*). Therefore, to prepare a zinc-bound form of this deletion mutant, 50 mM zinc acetate was added to all of the cryoprotectant solutions. Crystals were prepared for freezing as described above. Data were collected on frozen crystals as described above, and the structure of the apo form was used to solve this structure using molecular replacement. Even though zinc was not included in the initial refinement model, it was immediately apparent that zinc was bound and that there were concomitant conformational changes in the immediate vicinity of the bound zinc.

Table 3: Data Collection and Refinement Statistics[a]

	zinc bound	apo
PDB code	2OV3	2OV1
Data Collection		
space group	$C222_1$	$C222_1$
cell dimensions		
a, *b*, *c* (Å)	62.33, 76.98, 127.31	62.58, 76.50, 127.15
α, *β*, *γ* (deg)	90.0, 90.0, 90.0	90.00, 90.00, 90.00
resolution (Å)	50−2.4 (2.50−2.40)	50−2.5 (2.55−2.50)
R_{sym}	5.55 (29.7)	8.88 (28.5)
$I/\sigma I$	16.9 (3.4)	9.0 (3.3)
completeness (%)	92.8 (63.1)	96.1 (76.2)
redundancy	3.4 (2.0)	3.0 (1.2)
Refinement		
resolution (Å)	50−2.4 (2.49−2.40)	50−2.5 (2.59−2.5)
no. of reflections	10719	10189
R_{work}/R_{free} (%)	22.7/27.5 (21.0/26.3)	21.7/24.8 (23.9/28.0)
no. of atoms		
protein	2020	2020
ligands (Zn)	1	0
water	102	101
B-factors (Å^2)		
protein	26.2	28.8
ligands (Zn)	24.3	N/A
water	25.6	23.5
rms deviations		
bond lengths (Å)	0.0071	0.0074
bond angles (deg)	1.25	1.31
Ramachandran analysis		
most favored (%)	92.5	94.3
additionally allowed (%)	7.5	5.7
generously allowed (%)	0.0	0.0
disallowed (%)	0.0	0.0

[a] The highest resolution shell is shown in parentheses.

Isothermal Titration Calorimetry (ITC). Samples of ZnuA that had been stripped of zinc were dialyzed against 50 mM Tris buffer, pH 7.0, and 100 mM NaCl and loaded to the Superose 6 (Pharmacia Biotech) column preequilibrated with degassed buffer (100 mM Tris, pH 7.0, 100 mM NaCl).

ITC measurements were carried out on a MicroCal VP-ITC titration calorimeter (MicroCal, Inc.). Zinc chloride was dissolved in the same degassed buffer that the proteins were dialyzed against, and protein concentration was adjusted to 1−3 mM. The native and mutant forms of ZunA were thoroughly degassed before each titration. The protein samples ranging in concentrations from 0.02 to 0.035 mM were placed in the reaction cell, and the reference cell was filled with deionized water. For full-length ZnuA, 0.031 mM protein was placed in the cell, and 2 mM zinc chloride was used in the injection syringe. For Δ138−173 ZnuA, 0.0265 mM protein and 2 mM zinc cloride were used in measurement. Finally, for the Δ158−173 ZnuA experiments, 0.030 mM protein was placed in the cell, and 1 mM zinc chloride was used in the injection syringe.

All titrations were performed at 30 °C. After the temperature was equilibrated, 240 successive injections of the indicated zinc solution were made into the reaction cell in 10 μL while stirring at 260 rpm to ensure a complete

equilibration. The resulting heat of reaction was measured in 29 consecutive injections. Control experiments to determine the heat absorbed due to dilution of the zinc solution were carried out with identical injections in the absence of protein. These values were then used to normalize the ZnuA binding data. The titration data were curve-fitted to models that assumed either one or two classes of noninteracting binding sites using a nonlinear least-squares algorithm in the MicroCal Origin software package. The binding enthalpy change ΔH, association constant K_a, and the binding stoichiometry n were all refined during the least-squares minimization process. These studies were performed several times and yielded results within the error of curve fitting shown here.

RESULTS

In our previous report (*14*), we noted that the solute binding domains of the ABC zinc transporters differed from other divalent cationic transporters with regard to a distinctive loop starting at residue ~140 that was rich in acidic and histidine residues. While the length of this loop was significantly different among the various zinc transporters, the general amino acid compositions of these loops were very similar. This entire loop (residues 138−173) was disordered in the X-ray crystal structure. Since such residues are known for their zinc binding capabilities, we hypothesized that this loop might somehow facilitate the binding of zinc to the high-affinity site in the cleft between the two domains.

To dissect the possible role of this loop with regard to zinc binding to the high-affinity site, two constructs were created (Table 2). The first construct represented a "half-loop" deletion where residues 158−173 were replaced with a shorter PYTDK linker (called Δ158−173 ZnuA). The second construct (called Δ138−173 ZnuA) replaced the entire flexible loop with the much shorter loop (PGRL) that is found in other cluster 9 ABC solute binding domains. While both proteins expressed to relatively high levels and were readily purified, crystals were only obtained with the full loop deletion mutant (Δ138−173 ZnuA).

The structure was determined by molecular replacement methods using the structure of the full-length ZnuA. It was immediately apparent that the relative orientation of the two domains was significantly different than those of full-length ZnuA (Figure 1). For the alignment shown here, the least-squares refinement routine in MolViewX (*21*) was used. Using a distance cutoff of 1.5 Å during refinement of the alignment, 231 residues yielded a root mean square difference of 0.45 Å between the two structures. It should be noted that the fitting process was not biased toward the lower domain but rather used all residues within the 1.5 Å cutoff distance. It is clear that the structure of the protein main chain leading into and out of the flexible loop appears to be unchanged by the deletion (arrow A). When the zinc binding pocket of Δ138−173 ZnuA was further examined, it was apparent that zinc was not bound (Figures 2 and 3). It was possible that the structural differences were due to the deletion of flexible loop, the lack of bound zinc, or crystal contacts. If any of these possibilities were true, then it might be possible that zinc could not bind to ZnuA while in this crystal lattice.

To test for this possibility, crystals of Δ138−173 ZnuA were soaked in zinc acetate. In spite of the fact that zinc acetate in solution is actually chelated zinc and that the crystals are grown in, and stabilized by, high concentrations of ammonium sulfate, Δ138−173 ZnuA was able to bind zinc (Figures 2 and 3). What was particularly striking was that the backbone conformation of Δ138−173 ZnuA did not change significantly upon zinc binding. Again, using MolViewX and a 1.5 Å cutoff distance for the alignment refinement, 255 residues yielded a main chain root mean square difference of 0.28 Å between the two structures. This suggests that the zinc binding site remains fixed while the domains of the whole protein are rather plastic. Indeed, as shown in Figure 4, when the wt ZnuA is overlaid with Δ138−173 ZnuA, the residues in the zinc binding site are essentially identical. This suggests that the zinc binding environment is unaffected by either the loop deletion or the differences in domain conformations.

It is apparent that the absence of zinc is not responsible for the differences in the domain orientations. Therefore, it seems more likely that crystal packing is causing the differences in protein conformation. To examine this further, Figure 5 shows the crystal contacts of wt ZnuA versus Δ138−173 ZnuA. In wt ZnuA, the contacts are mostly mediated by antiparallel interactions of the α-helices running along the back of the protein (arrow A) and by side-to-side contacts. In Δ138−173 ZnuA, the back α-helix from one makes close contacts with the front face in the adjacent protein (arrow B), and the back α-helices contact each other in a perpendicular manner (arrow C). Since this region of the front face of the protein is exactly the area most different in conformation compared to wt ZnuA (Figure 1A), it seems most likely that the structural differences between wt ZnuA and Δ138−173 ZnuA are due to crystal packing forces and are not due to either zinc binding or the deletion of the flexible loop. It seems also likely that these differences in crystal packing are due to the large (35 residues) disordered loop that has now been deleted in Δ138−173 ZnuA.

While the backbone of Δ138−173 ZnuA remains largely unaffected by zinc binding, there are striking changes in the zinc binding site (Figures 2−4). Zinc bound to Δ138−173 ZnuA is essentially identical to that observed in wt ZnuA even with regard to the water molecule associated with zinc, and compared to the apo form, relatively few water molecules are present elsewhere in this metal binding pocket. When zinc is released, two of the three histidines (H83 and H243) sweep out of the binding pocket while H179 remains in the same orientation. The metal−H179 interaction is replaced by a hydrogen bond with a new water molecule. In the presence of zinc, H243 is hydrogen bonded to both E261 and the zinc atom. In the absence of zinc, the side chains of H243 and E261 move out of the metal binding pocket and maintain that hydrogen bond. E290 moves in to replace the H243−zinc hydrogen bond. In this new orientation, E290 also forms a hydrogen bond with S245. As H83 leaves the metal binding pocket, D81 moves in with two associated water molecules. Overall, the removal of zinc from the binding pocket causes a marked increase in hydration.

Our previous model suggested that the flexible loop contained at least one relatively low-affinity zinc binding site that might facilitate the loading of zinc to the high-affinity site at low zinc concentrations. From the structural studies presented here it is clear that the high-affinity zinc binding site is unperturbed by the deletion of the flexible

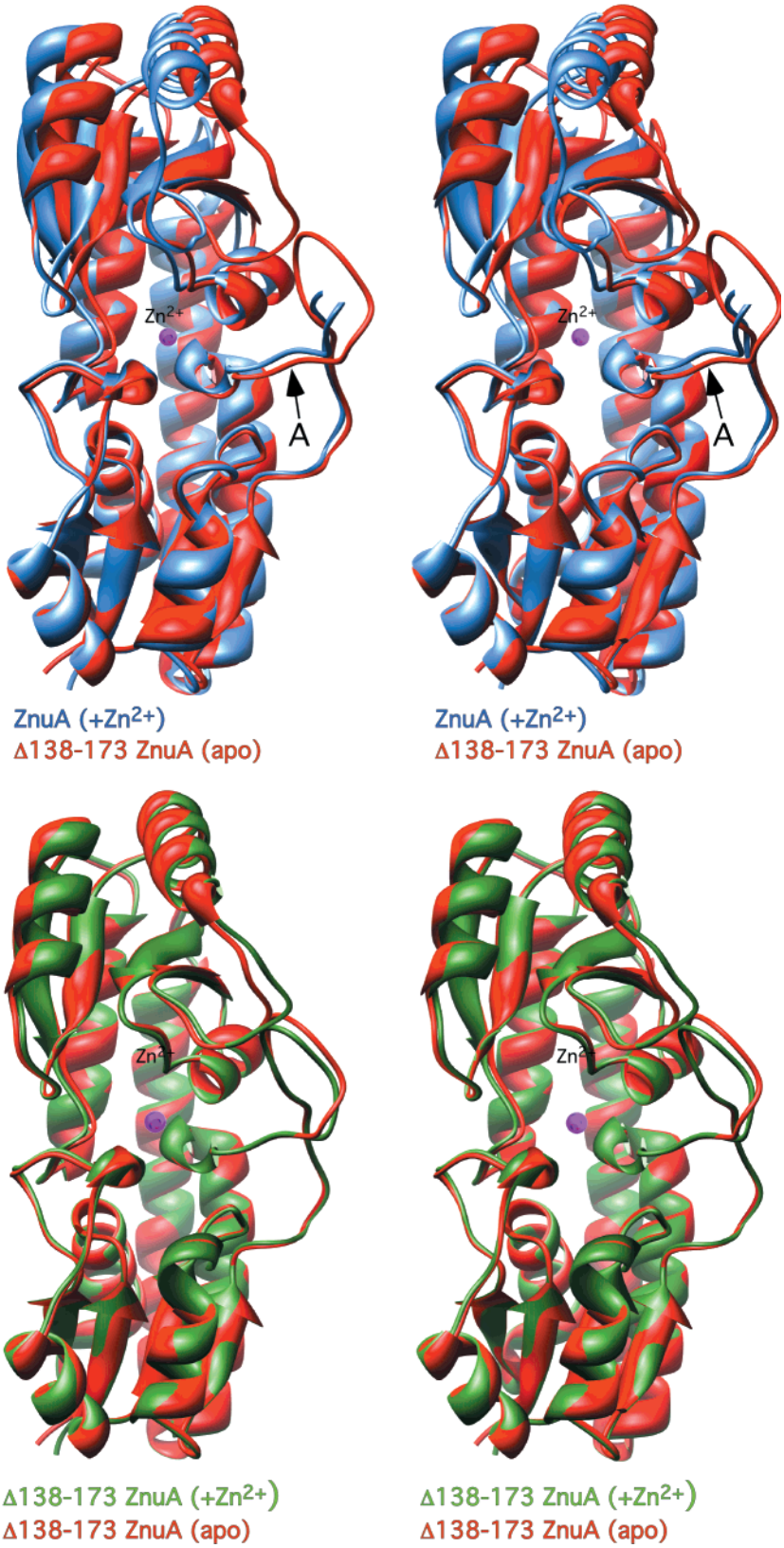

FIGURE 1: Structures of apo and zinc-bound Δ138−173 ZnuA compared to wild-type ZnuA. The top stereo ribbon diagram shows a comparison of the full-length ZnuA (blue) with the apo form of Δ138−173 ZnuA (red). The bound zinc in the wild-type ZnuA structure is represented by the mauve sphere. Arrow A highlights the carboxyl end of the flexible loop. Note that the deletion does not affect the conformation of the polypeptide leading into, or returning from, this flexible region.

loop. To further examine the possible role that the flexible loop plays in zinc binding, isothermal titration calorimetry was used to examine zinc binding to the wild-type, Δ158−173, and Δ138−173 forms of ZnuA (Figure 6).

The binding of zinc to wild-type ZnuA cannot be described by a single class of sites model. As shown in Figure 6 and summarized in Table 4, the binding fits well to a model with two classes of sites with disassociation constants of ~10 and

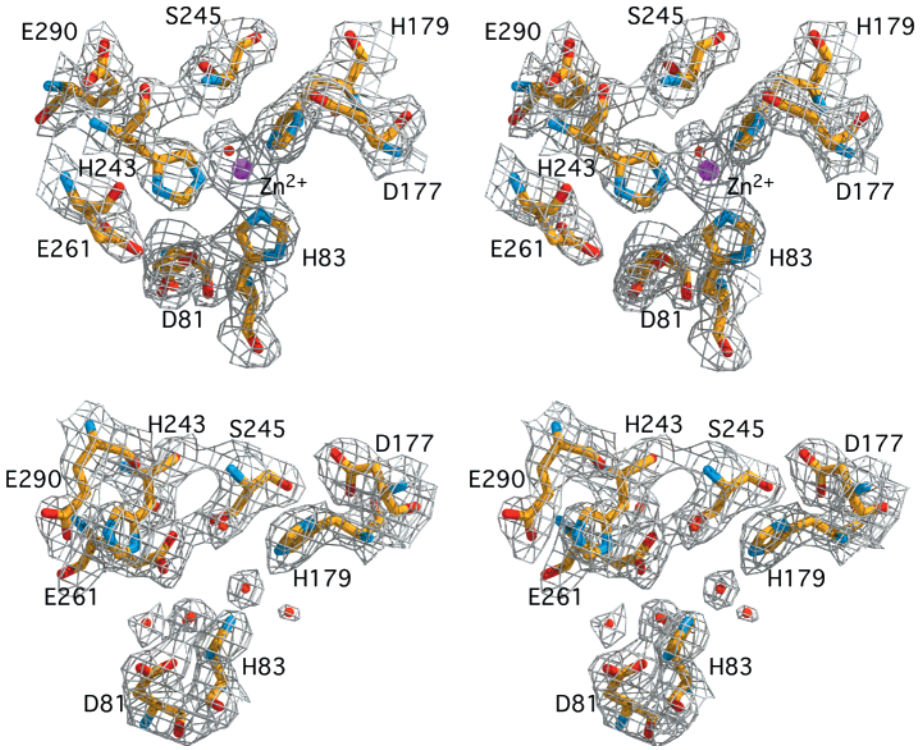

FIGURE 2: Electron density of the Δ138−173 ZnuA zinc binding pocket. The top figure shows the electron density of the zinc-bound form of Δ138−173 ZnuA, and the bottom figure shows the same area in the apo form of Δ138−173 ZnuA. The view is approximately the same as used in Figure 1 with a focus on the cleft between the two domains. The stick figure is colored according to atom type: nitrogen is in blue, carbon is in yellow, and oxygen is in red. The bound zinc is shown as a mauve sphere, and bound water molecules are represented by red spheres. The electron density for both figures is represented by the gray cage and was calculated to 2.5 Å at a contour of 1σ. It should be noted that, assuming an occupancy of 1.0, the *B* value for the bound zinc is the same as the surrounding ligating side chains (~24 Å^2).

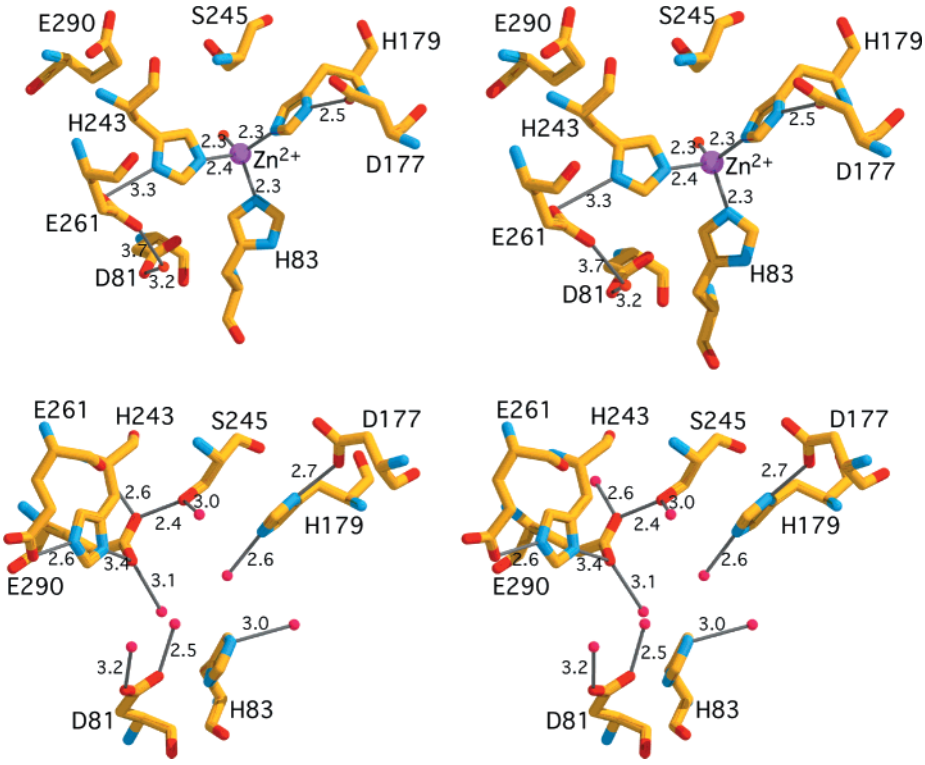

FIGURE 3: Chemical interactions in the Δ138−173 ZnuA zinc binding pocket. The orientation and color scheme is the same as in Figure 2. The top figure is the zinc-bound form of Δ138−173 ZnuA, and the bottom is the apo form.

10000 nM. The number of zinc molecules bound per class of sites and the enthalpies for each class of sites are linked parameters. To try to compensate for this, the ratio of the low-affinity sites to high-affinity sites was compared. For wild type, the ratio of low affinity to high affinity is 3. These results are in contrast to the Δ138−173 form of ZnuA. Here,

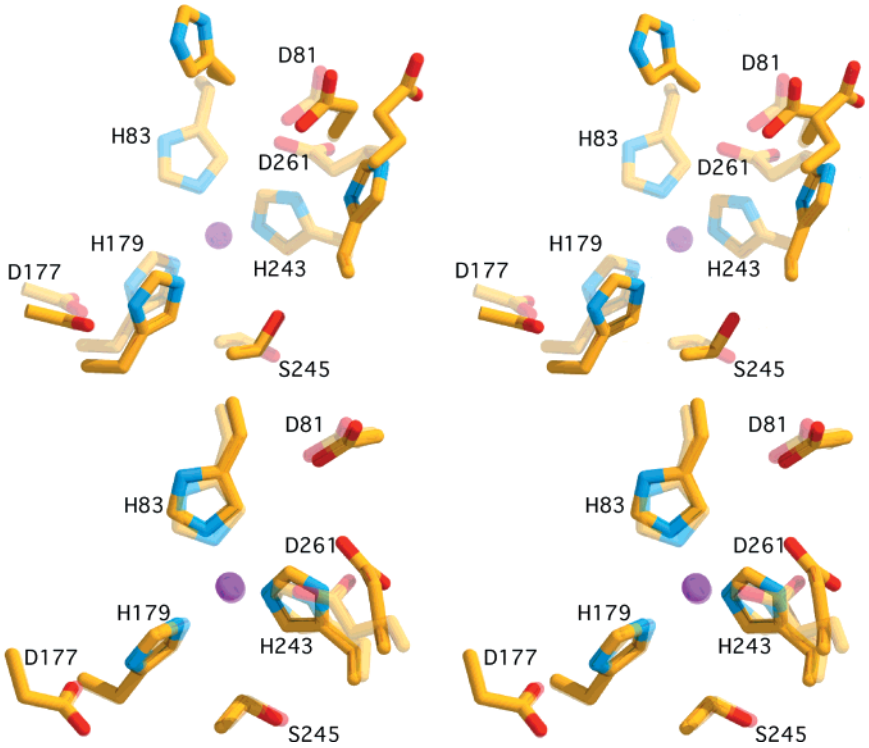

FIGURE 4: Comparison of the ZnuA−zinc interactions. Shown here are the structures of apo Δ138−173 ZnuA (top) and zinc-bound Δ138−173 ZnuA aligned to the zinc-bound, full-length form of ZnuA. The orientation and coloring is the same as used in Figures 2 and 3. The structure of the full-length form is represented by the transparent stick figure. Note that the changes in the zinc binding site upon zinc release are by far larger than those observed between the full-length and truncated forms.

the data are very well described by the model assuming only a single class of zinc binding sites. When the error of the curve fitting is accounted for, the binding constant for this one site is very close to that of the high-affinity site of wild-type ZnuA. Therefore, this demonstrates that the intrinsic affinity for zinc binding to the high-affinity site is relatively unaffected by the deletion of the flexible loop. This also suggests that the loop itself does not appear to facilitate the acquisition of zinc in the high-affinity site at least in vitro. From the chemical nature of the flexible loop, it seems likely that there are multiple binding sites for zinc on the flexible loop. Indeed, when half of the loop is deleted (Δ158−173 ZnuA), there are still two classes of binding sites, but now the ratio of low- to high-affinity sites has decreased to approximately 1. Further, the association constants for both classes of sites are consistent with both wild-type and Δ138−173 ZnuA. Therefore, the data suggest that the loop has multiple binding sites for zinc but that the affinity of these sites for zinc are 2−3 orders of magnitude weaker than the high-affinity site. Further, neither full nor partial deletion of this loop appears to have significant effects on the ability of the high-affinity site to bind zinc in vitro.

DISCUSSION

Previously, the structure of a homologous metal binding protein, TroA, was determined in the presence (*9*) and absence (*10*) of bound metal. In this case, it was suggested that, upon the release of bound metal, the metal binding site "collapses" such that D66 (TroA sequence) shifts toward one of the chelating histidines, H68. It was suggested that this, in turn, caused the imidazole ring of H68 to flip and facilitates the release of bound metal. It should be noted that these two forms of TroA crystallized in two different space groups with inherently different crystal lattice contacts.

The effects of metal binding and release are quite different in the case of Δ138−173 ZnuA. In this case, the apo and metal-bound forms were in the same crystal lattice with exactly the same protein contacts. Here, the domains did not appear to move significantly upon zinc binding or release. However, there was a rather large conformational difference between the full-length and Δ138−173 mutant form of ZnuA. While it might be suggested that the deletion itself caused the conformational difference, this seems highly unlikely since the structure of the ZnuA at either side of the flexible loop was unaffected by the truncation (see arrow A, Figure 1). Second, the truncation did not have a significant effect on the high-affinity zinc binding site (Figure 6 and Table 4). Indeed, data from the soaking experiments show that the crystals of the apo form of Δ138−173 ZnuA are able to pull the zinc ion out of the acetate shell in a sulfate-rich crystallization mother liquor. This suggests that the crystalline form of ZnuA also binds zinc with high affinity, and therefore any conformational restriction of the domain orientations due to crystal packing does not prevent metal binding. It is highly likely that the conformational differences between the structures of full-length ZnuA and Δ138−173 ZnuA are due to crystal packing forces (Figure 5). Here, the areas of largest conformational changes directly correspond to differences in crystal packing contacts. This suggests that ZnuA is more plastic than previously thought and yet the zinc binding site itself appears to be mostly unaffected by these conformational changes (Figure 4).

There are, however, a number of large changes in side chains lining the zinc binding pocket upon the release of

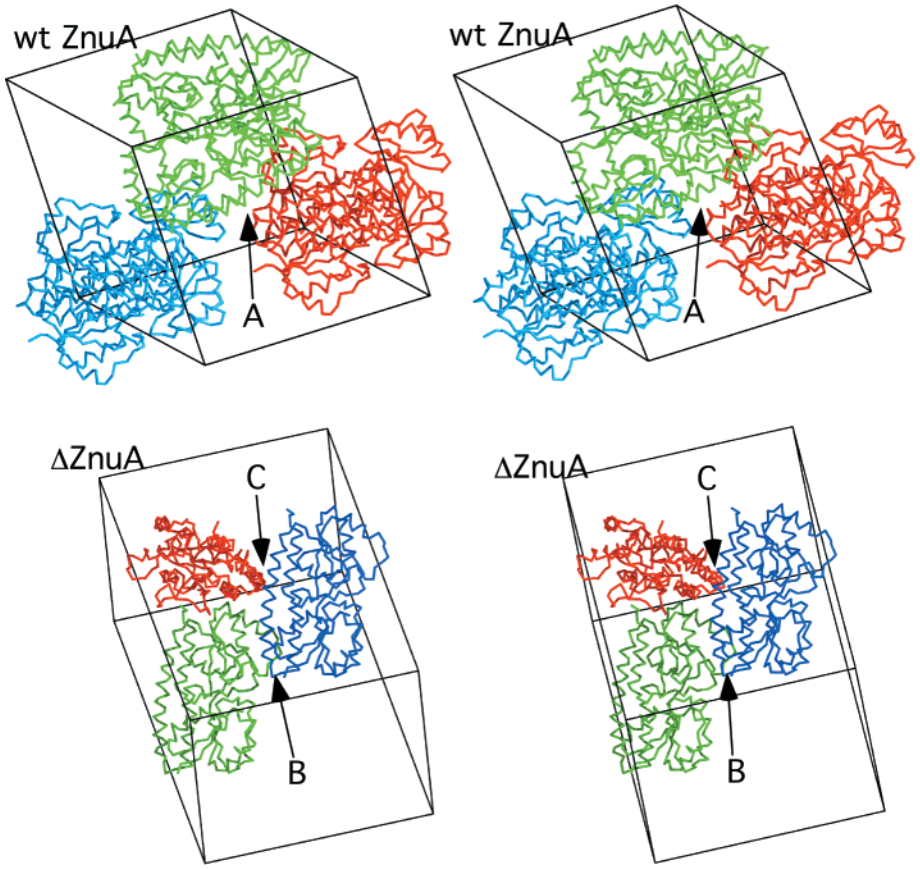

FIGURE 5: Differences in crystal packing between crystals of full-length and Δ138−173 ZnuA. Shown here are portions of the crystalline arrays of the full-length ZnuA (top) and Δ138−173 ZnuA (bottom). Three copies of ZnuA are colored red, green, and blue. One of the unit cell boundaries is represented by black lines. Arrow A denotes the contact found in crystals of the full-length protein mediated by the long α-helices running along the back of the protein. Arrow B notes the contact found in the Δ138−173 ZnuA crystals between the back α-helix of one and the "top domain" of another. The top domain is the portion of the structure that shows the largest deformation compared to the full-length protein. Arrow C notes that, in contrast to the full-length protein, the α-helices are not making antiparallel contact but instead are perpendicular to each other.

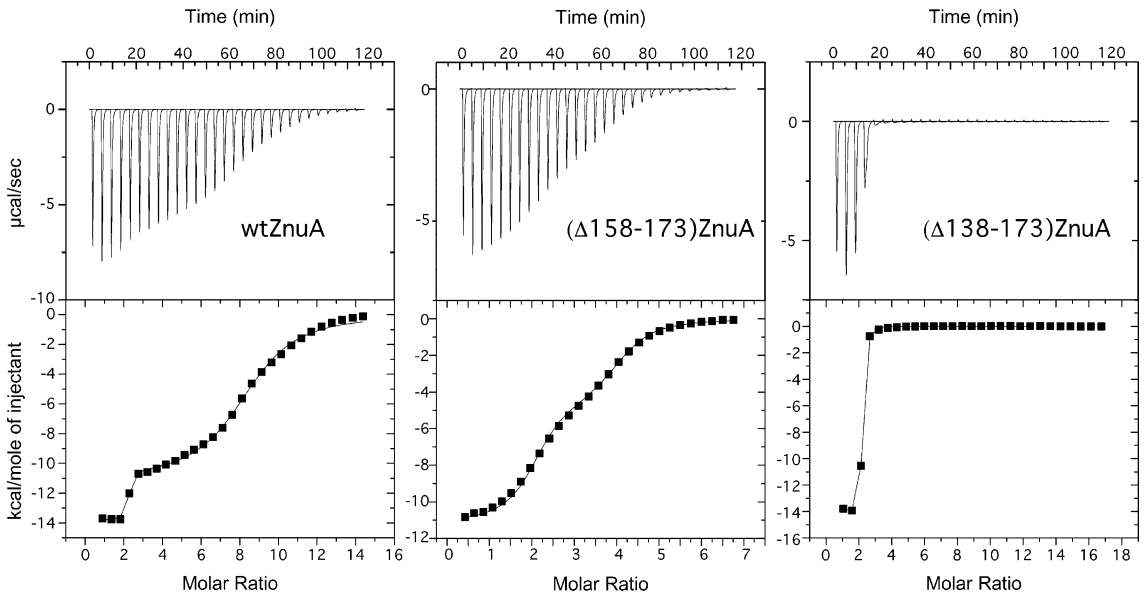

FIGURE 6: Isothermal titration calorimetry analysis of zinc binding. Shown here are the ITC results of zinc binding to full-length (left), Δ138−173, and Δ158−173 forms of ZnuA. The top figures show the raw data, and the bottom figures show the same data along with the curve fitting results. The curve fitting results are summarized in Table 4.

zinc. In the case of TroA, it was suggested that the release of metal is facilitated by the rather subtle rotation of the H68 imidazole ring. This is not the case with ZnuA. Instead, only one histidine remains in its original conformation (H179) while the other two (H83 and H243) rotate out of the metal binding pocket and are replaced by a number of water molecules and acidic residues. Since zinc can bind relatively well to two histidines, perhaps this movement is necessary

Table 4: Isothermal Titration Calorimetry Analysis

ZnuA	model	site	K_a (M^{-1})	K_d (nM)	no. bound
wt	2-site	1	$1.4 \times 10^8 \pm 1.8 \times 10^8$	7.3	2.0 ± 0.04
		2	$1.1 \times 10^5 \pm 8.9 \times 10^3$	8770	6.3 ± 0.06
Δ158−173	2-site	1	$1.0 \times 10^7 \pm 6.3 \times 10^5$	99	2.0 ± 0.02
		2	$3.7 \times 10^5 \pm 2.6 \times 10^4$	2740	2.0 ± 0.02
Δ138−173	1-site	1	$1.4 \times 10^7 \pm 1.3 \times 10^6$	70	2.0 ± 0.004

to facilitate zinc release. Recent studies compared the structure of zinc-bound *E. coli* ZnuA with other cluster 9 solute binding domains and suggested that there are concerted changes in the protein that they called "partial domain slippage" associated with metal release and binding (*15*). However, these predicted changes are not observed here when comparing the structures of the metal-bound and apo forms of the same solute binding domain. Indeed, the largest differences in the domain orientation appear to stem from crystal packing forces rather than metal binding and release. It remains unclear what triggers zinc release to the ZnuB pore. The apparently plasticity of ZnuA implies that, unlike other ABC transporters, the transmembrane pore may not be signaling metal release via imposition of conformational changes in the solute binding domain. Perhaps for this class of ABC transporters, zinc release from ZnuA is a passive event with the intracellular ATPase driving large conformational changes in the ZnuB pore more so than ZnuA. For example, the ATPase may act on ZnuB to open a binding site with higher affinity than that found in ZnuA or a direct opening to the cytoplasm where the free zinc concentration is extremely low.

The results presented here begin to narrow the possible functions of the flexible loop that is rich in histidine and acidic residues (residues 138−173). This feature is found in all of the cluster 9 zinc transporters and yet was completely disordered in the structure of full-length ZnuA (*14*). It is now clear that this loop likely has multiple zinc binding sites with at least 100-fold weaker binding constants than the high-affinity site. Further, the deletion of this highly mobile loop does not affect the remaining ZnuA structure nor does it alter the binding of zinc to the high-affinity site. We had previously suggested that the loop might "chaperone" zinc to the high-affinity site perhaps by increasing the pool of zinc around the high-affinity site. However, at least in vitro, deletion of the loop does not seem to affect zinc binding.

It is possible that this loop is playing a regulatory role in ZnuABC-mediated transport. High levels of zinc are toxic to the cell, and therefore the intracellular concentrations need to be strictly regulated. To this end, there is transcriptional regulation of the *znuabc* operon. However, transcriptional control does not address the potential problem of rapid increases in zinc concentration in the extracellular milieu that might overwhelm the cell before transcriptional regulation can rectify the situation. It is possible that this low-affinity zinc binding loop is actually a "sensor". We propose that, at very low concentrations of zinc, the only location that zinc can bind is to the high-affinity site. From atomic absorption analysis of full-length ZnuA (data not shown) prepared in low zinc conditions, in the manner described in our previous studies (*14*), there is approximately one zinc atom bound per protein. The structure of this form places that zinc in the high-affinity site with an entirely disordered 138−173 loop. It may be that, at concentrations 100-fold higher than that needed for binding to the high-affinity site, zinc associates with the flexible loop and may actually lend structure to at least portions of the loop. This might block zinc transport by preventing association of ZnuA with ZnuB. It could even be that zinc associating with the loop could aggregate two or more copies of ZnuA and block zinc transport, akin to the aggregation commonly seen with His-tagged protein expression.

Interestingly, the C-terminal region of the ATPase domain that drives the import of zinc is also rich in histidine and acidic amino acids. The C-terminus of ZnuC (the ATPase of the ZnuABC system) is much longer than that from the manganese transport system, MntA, and is similar in length and chemical character to the flexible loop found in ZnuA. The full-length loop in ZnuA is ~36 residues long with 8 histidines and 12 acidic amino acids whereas the C-terminus in ZnuC is about the same length with 6 histidines and 5 acidic residues. Therefore, it is tempting to speculate that the C-terminal region of ZnuC binds metal in a manner akin to the long flexible loop in ZnuA and regulates the ATPase activity on the cytosolic side of the ABC transporter. At high cytosolic concentrations of zinc, metal may bind to the C-terminus of ZnuC and inhibit further import of zinc. It seems logical that a high-affinity transport system would have sensors on both sides of the membrane to afford a rapid response to excessive zinc concentrations. However, it should be noted that a similar regulatory role was suggested for a cluster of three histidines in a cytosolic domain of the zinc transporter, Zrt1 (*22*). Subsequent mutational analysis demonstrated that these residues were, in fact, not required for inactivation of the transporter (*23*).

Nevertheless, the data presented here suggest that both models can be directly tested. We now know that the flexible zinc binding loop can be removed from ZnuA without any deleterious effect on the high-affinity site. According to the original model, if the flexible loop is used to chaperone zinc into the high-affinity site by acquiring it either from other proteins or from solution, then replacing wild-type ZnuA with the Δ158−173 deletion should impair cellular growth in low zinc media. Alternatively, if the loop acts to allosterically inhibit zinc uptake at high zinc concentrations, then one would expect that the cells would become more sensitive to high zinc concentrations. Such studies are currently underway.

ACKNOWLEDGMENT

MolView (*21*) was used for the creation of Figures 2−5, and Chimera (*24*) was used to make Figure 1.

REFERENCES

1. Claverys, J. P. (2001) A new family of high-affinity ABC manganese and zinc permeases, *Res. Microbiol. 152*, 231−243.
2. Hantke, K. (2001) Bacterial zinc transporters and regulators, *Biometals 14*, 239−249.
3. Grass, G., Wong, M. D., Rosen, B. P., Smith, R. L., and Rensing, C. (2002) ZupT is a Zn(II) uptake system in *Escherichia coli*, *J. Bacteriol. 184*, 864−866.
4. Bartsevich, V. V., and Pakrasi, H. B. (1996) Manganese transport in the cyanobacterium *Synechocystis* sp. PCC 6803, *J. Biol. Chem. 271*, 26057−26061.
5. Bouige, P., Laurent, D., Piloyan, L., and Dassa, E. (2002) Phylogenetic and functional classification of ATP-binding cassette (ABC) systems, *Curr. Protein Pept. Sci. 3*, 541−559.

6. Pakrasi, H. B., Ogawa, T., and Bhattacharyya-Pakrasi, M. (2001) Transport of metals: a key process in oxygenic photosynthesis, in *Regulation of Photosynthesis* (Aro, E.-M., and Andersson, B., Eds.) pp 253−264, Kluwer Academic Publishers, Dordrecht, The Netherlands.
7. Dintilhac, A., Alloing, G., Granadel, C., and Claverys, J. P. (1997) Competence and virulence of *Streptococcus pneumoniae*: Adc and PsaA mutants exhibit a requirement for Zn and Mn resulting from inactivation of putative ABC metal permeases, *Mol. Microbiol. 25*, 727−739.
8. Deka, R. K., Lee, Y. H., Hagman, K. E., Shevchenko, D., Lingwood, C. A., Hasemann, C. A., Norgard, M. V., and Radolf, J. D. (1999) Physicochemical evidence that *Treponema pallidum* TroA is a zinc-containing metalloprotein that lacks porin-like structure, *J. Bacteriol. 181*, 4420−4423.
9. Lee, Y.-H., Deka, R., Norgard, M. V., Radolf, J. D., and Hasemann, C. A. (1999) *Treponema pallidum* TroA is a periplasmic zinc-binding protein with α helical backbone, *Nat. Struct. Biol. 6*, 628−633.
10. Lee, Y.-H., Dorwart, M. R., Hazlett, K. R. O., Deka, R. K., Norgard, M. V., Radolf, J. D., and Hasemann, C. A. (2002) The crystal structure of a Zn(II)-free *Troponema pallidum* TroA, a periplasmic metal-binding protein, reveals a closed conformation, *J. Bacteriol. 184*, 2300−2304.
11. Patzer, S. I., and Hantke, K. (1998) The ZnuABC high-affinity zinc uptake system and its regulator Zur in *Escherichia coli*, *Mol. Microbiol. 28*, 1199−1210.
12. Chen, C. Y., and Morse, S. A. (2001) Identification and characterization of a high-affinity zinc uptake system in *Neisseria gonorrhoeae*, *FEMS Microbiol. Lett. 202*, 67−71.
13. Lewis, D. A., Klesney-Tait, J., Lumbley, S. R., Ward, C. K., Latimer, J. L., Ison, C. A., and Hansen, E. J. (1999) Identification of the znuA-encoded periplasmic zinc transport protein of *Haemophilus ducreyi*, *Infect. Immun. 67*, 5060−5068.
14. Banerjee, S., Wei, B., Bhattacharyya-Pakrasi, M., Pakrasi, H. B., and Smith, T. J. (2003) Structural determinants of metal specificity in the zinc transport protein ZnuA from *Synechocystis* 6803, *J. Mol. Biol. 333*, 1061−1069.
15. Chandra, B. R., Yogavel, M., and Sharma, A. (2007) Structural analysis of ABC-family periplasmic zinc binding protein provides new insights into mechanism of ligand uptake and release, *J. Mol. Biol. 367*, 970−982.
16. Li, H., and Jogl, G. (2007) Crystal structure of the zinc-binding transport protein ZnuA from *Escherichia coli* reveals an unexpected variation in metal coordination, *J. Mol. Biol. 368*, 1358−1366.
17. Vagin, A., and Teplyakov, A. (1997) MOLREP: an automated program for molecular replacement, *J. Appl. Crystallogr. 30*, 1022−1025.
18. Brunger, A. T., Adams, P. D., Clore, G. M., Gros, P., Grosse-Kunstleve, R. W., Jiang, J.-S., Kuszewski, J., Nilges, N., Pannu, N. S., Read, R. J., Rice, L. M., Simonson, T., and Warren, G. L. (1998) Crystallography & NMR system (CNS): A new software system for macromolecular structure determination, *Acta Crystallogr. D 54*, 905−921.
19. Jones, T. A. (1982) *A Graphics Model Building and Refinement System for Macromolecules*, Clarendon Press, Oxford.
20. Laskowski, R. A., MacArthur, M. W., Moss, D. S., and Thornton, J. M. (1993) PROCHECK: a program to check the sterochemical quality of protein structures, *J. Appl. Crystallogr. 26*, 283−291.
21. Smith, T. J. (2004) MolViewX: a molecular visualization program for the Macintosh OS X system, *J. Appl. Crystallogr. 37*, 654−657.
22. Gitan, R. S., and Eide, D. J. (2000) Zinc-regulated ubiquitin conjugation signals endocytosis of the yeast ZRT1 zinc transporter, *Biochem. J. 346*, 329−336.
23. Gitan, R. S., Shababi, M., Kramer, M., and Eide, D. J. (2003) A cytosolic domain of the yeast Zrt1 zinc transporter is required for its post-translational inactivation in response to zinc and cadmium, *J. Biol. Chem. 278*, 39558−39564.
24. Pettersen, E. F., Goddard, T. D., Huang, C. C., Couch, G. S., Greenblatt, D. M., Meng, E. C., and Ferrin, T. E. (2004) UCSF chimera−A visualization system for exploratory research and analysis, *J. Comput. Chem. 25*, 1605−1612.

BI700763W